ELSEVIER

Catalysis Today 44 (1998) 293–300

CATALYSIS TODAY

Molybdenum ZSM-5 zeolite catalysts for the conversion of methane to benzene

Jun-Zhong Zhang[a], Mervyn A. Long[a], Russell F. Howe[b,*]

[a]*Department of Inorganic Chemistry, University of New South Wales, Sydney, NSW 2052, Australia*
[b]*Department of Physical Chemistry, University of New South Wales, Sydney, NSW 2052, Australia*

Abstract

This paper describes characterization studies of Mo-HZSM-5 zeolite catalysts active for the non-oxidative conversion of methane to benzene. FTIR, ^{27}Al and ^{29}Si NMR evidence is presented for migration of molybdenum into the zeolite pores during catalyst calcination at high temperatures. Mo K-edge EXAFS confirms that calcination produces highly dispersed oxomolybdenum or molybdate species which are converted to a molybdenum carbide phase under reaction conditions. Factors determining catalyst performance are discussed.

Keywords: Molybdenum; ZSM-5; Methane; EXAFS

1. Introduction

The non-oxidative conversion of methane to benzene has recently attracted considerable attention [1–17]. There is general agreement that over molybdenum loaded HZSM-5 zeolite catalysts methane conversions of up to 8% with selectivities to benzene of 70% or higher can be obtained at reaction temperatures of 700–800°C. These values approach the calculated thermodynamic equilibrium conversions (e.g. 12% methane conversion at 700°C, to equimolar benzene and naphthalene [14]).

There are several important aspects of this reaction which have been investigated following its initial discovery [1]. Firstly, the intrinsic activity of the catalyst is rather low. Maximum methane conversions have been achieved only at very low space velocities (e.g. 7% conversion at GHSV=800 h^{-1} [14]). This has prompted a number of groups to investigate promotion of the catalyst by incorporating other components. Some modest success in enhancing activity has been obtained by promotion with, for e.g., W, Zr, Ru [5,10,16] and Fe [17], although the effects reported are not large.

A second issue of interest has been the reaction mechanism. Heterolytic dissociation of the C–H bond in methane on high oxidation state molybdenum sites to form a molybdenum carbene species, which subsequently dimerizes to ethylene was proposed by Guo and coworkers [3,5,10,11], the ethylene then reacting over HZSM-5 acid sites to generate aromatics. Chen et al. [4], on the other hand, proposed that methyl radicals were a key initial intermediate in the mechanism. Solymosi et al. [2] suggested that partially reduced molybdenum species, probably Mo^{4+}, were responsible for methane activation, whereas Lunsford and coworkers [7,14] showed convincingly that highly

*Corresponding author. Tel.: 00 61 2 9385 4674; fax: 00 61 2 9385 6141; e-mail: r.howe@unsw.edu.au

0920-5861/98/$32.00
PII S0920-5861(98)00202-8

reduced molybdenum species, probably molybdenum carbide, were dominant in active catalysts.

Catalyst stability and lifetime is a third area of concern with this reaction. Coke formation causes a gradual decline in methane conversion to benzene with time on stream. Ichikawa and coworkers [17] recently reported that catalyst promotion with Fe suppressed coke formation, although no catalyst lifetime data were given.

We have taken the view that it is necessary to understand in much greater detail the chemistry of the catalyst preparation, activation and deactivation if progress is to be made in understanding the reaction mechanism and in developing improved versions of this potentially important catalytic process for upgrading natural gas. We report here characterization studies of the unpromoted Mo-HZSM-5 zeolite catalyst which confirm the formation of a molybdenum carbide phase in the active catalysts, and which provide more evidence of a specific interaction of molybdenum and Brønsted acid sites within the zeolite pores.

2. Experimental

Catalysts were prepared from a commercial HZSM5 zeolite (PQ corporation, SiO_2/Al_2O_3=35). The zeolite was impregnated with an aqueous solution containing an appropriate concentration of ammonium heptamolybdate (Ajax), then dried at 110°C for 12 h (denoted as a fresh catalyst) and then calcined either in flowing air or in flowing helium at 500–700°C for 1 h. Molybdenum carbide (β Mo_2C) was prepared by the method of Lee et al. [18], then passivated by treatment with oxygen. This passivation procedure produces a surface layer of molybdenum oxide without altering the X-ray diffraction pattern of the underlying carbide. Physical mixtures of molybdenum carbide and HZSM-5 were prepared under flowing nitrogen, but subsequent pelletization and loading into the reactor was performed in air. $Al_2(MoO_4)_3$ was prepared by firing a stoichiometric mixture of Al_2O_3 and $Na_2(MoO_4)_3$ as described by Harrison et al. [19].

Catalyst testing was undertaken in a fixed bed continuous flow microreactor comprising a 3 mm i.d. quartz tube containing 0.2 g of the catalyst. High purity methane was flowed through the reactor via a mass flow controller, and gaseous products sampled by an on-line GC (Poropak Q). A methane flow rate of 300 ml h^{-1} was used, corresponding to a GHSV of 1500 h^{-1}.

^{27}Al and ^{29}Si MAS NMR spectra were recorded on a Bruker MSL300 spectrometer at 78.2 and 59.6 MHz, respectively. ^{27}Al spectra were measured at a spinning rate of 10 kHz using a 15° pulse width. ^{29}Si spectra were measured with a 90° pulse width at a spinning rate of 3 kHz, and kaolin was used as an external standard for both nuclei.

X-ray powder diffraction patterns were obtained with a Siemens D-500 diffractometer using Cu K_α radiation. XPS measurements were made on pressed wafers of catalysts with a Kratos XSAM800 instrument using unmonochromated Mg K_α X-rays. All binding energies were referenced to Si(2p)=103.4 eV.

Infrared spectra were measured from pressed wafers of catalysts mounted in an in situ flow cell, using a Bomem MB100 spectrometer with an MCT detector. Catalyst wafers were dehydrated by heating in flowing nitrogen to 673 K, then cooled to 373 K for recording the spectra. Acidity measurements were undertaken with pyridine, as described by Campbell et al. [20].

X-ray absorbtion spectra at the Mo K-edge were measured on BL20B at the Photon Factory, Japan, from pressed wafers of catalyst in transmission mode, using a Si(1 1 1) monochromator calibrated with Mo foil. Analysis of EXAFS data was undertaken using the XFIT and FEFF5.0 codes [21].

3. Results and discussion

3.1. Catalyst activity

Fig. 1 shows plots of methane conversion and selectivity to benzene and ethylene versus time on stream at 700°C for a 4 wt% Mo-HZSM-5 catalyst, a 4 wt% molybdenum Mo_2C:HZSM-5 mixture, and unsupported Mo_2C. The data for the Mo-HZSM-5 catalyst are similar to those reported previously by others. There is an initial induction period in the formation of hydrocarbon products; a maximum methane conversion of around 7% is achieved under these conditions with a selectivity to benzene of around 80%. The only other gaseous hydrocarbon product detected in large amounts is ethylene; traces

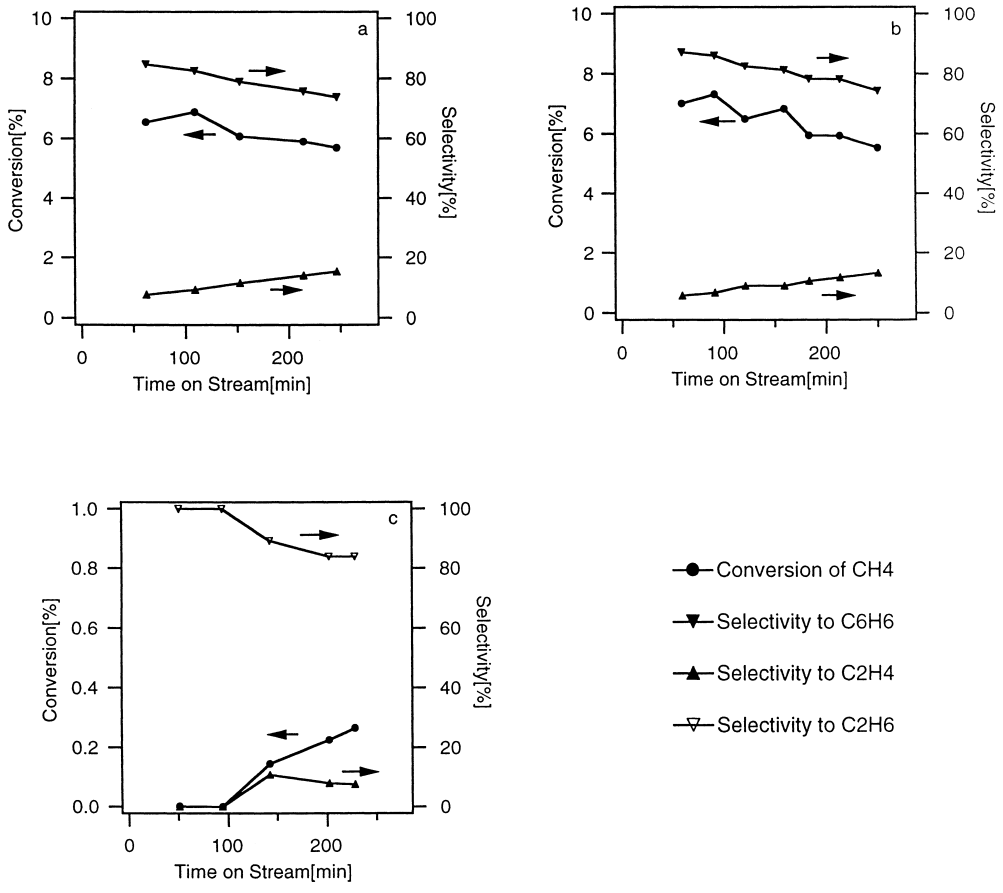

Fig. 1. Conversion of methane to hydrocarbon products and product selectivities at 700°C, GHSV=1500 h^{-1}, over: (a) 4% Mo-HZSM-5; (b) 4% molybdenum Mo_2C:HZSM-5 mixture; (c) unsupported Mo_2C.

of solid napthalene were observed at the exit of the reactor, but this product was not included in the selectivity calculations. Catalyst performance slowly deteriorated with time on stream; this gradual deactivation has been attributed to coke formation [14]. Identical performance was obtained from catalysts calcined in air or in helium at 700°C.

The activity of the catalyst prepared as a mixture of Mo_2C and HZSM-5 is similar to that of the impregnated catalyst (maximum methane conversion around 7%), the selectivities to benzene and ethylene are similar, and the catalyst slowly deactivated in a similar manner. Similar catalyst activity was achieved for the mixed catalysts calcined in air or in helium. Unsupported Mo_2C (calcined in helium), on the other hand, showed an initial very low activity which increased with time on stream (methane conversion around 0.2%), and gave ethane as the major product. Small amounts of ethylene were also formed, but no other hydrocarbon products (particularly benzene) were detected.

3.2. Catalyst characterization

X-ray powder diffraction measurements confirmed that all fresh and used zeolite catalysts retained the ZSM-5 structure. X-ray photoelectron spectra of fresh, calcined and used catalysts were similar to those reported by Lunsford and coworkers [14]. Freshly prepared catalysts showed a poorly resolved Mo 3d spin-orbit doublet at binding energies characteristic of Mo(VI) ($Mo(3d_{5/2})$=232.5 ev). Calcination did not

change the binding energy but did reduce the line widths of the two components. Used catalyst samples (removed from the reactor under nitrogen but exposed briefly to air during insertion into the instrument) showed the intense lower binding energy doublet ($Mo(3d_{5/2})$=228 eV) attributed by Lunsford and coworkers [14] to a molybdenum carbide phase. As shown in [14], the Mo 3d binding energy alone is not sufficient to distinguish between molybdenum carbide and molybdenum metal; this was done by observing also the C 1s signal characteristic of carbide, and deducing a stoichiometry close to that of Mo_2C. In our case, the oxidation of the molybdenum during sample transfer produced a mixture of higher oxidation states, and it was thus not possible to confirm absolutely the presence of Mo_2C.

Table 1 shows the results of XPS quantification of total molybdenum, silicon and aluminium in fresh, calcined and used catalysts. The near-surface Si:Al ratios of the fresh, calcined and used catalysts are similar to that obtained from bulk analysis indicating, little if any, migration of aluminium to or from the external surface of the zeolite. The near-surface Mo:Si ratio of the fresh catalyst is less than that of the bulk, which might at first be taken to indicate that molybdenum is adsorbed within the zeolite pores. This is unlikely however given the anionic nature of the heptamolybdate species. The alternative explanation (and that proposed by Lunsford and coworkers [14]) is that molybdenum is present on the external surface in the form of crystallites somewhat larger than the mean free path of the Mo 3d photoelectrons (16–17 Å).

On calcination, the near-surface Mo:Si ratio increases 5-fold. Spreading of molybdenum oxide on support surfaces during calcination is a well-documented phenomenon [22]; and will increase the Mo:Si ratio measured by XPS. The ratio observed for the 4% Mo-HZSM-5 catalyst after calcination at 973 K is however only twice that of the bulk, and much less than that expected for complete spreading on the external surface of the zeolite. We concur with the argument of Lunsford and coworkers [14] that during calcination molybdenum is migrating into the zeolite pores to some extent.

Table 1
Surface composition of Mo-HZSM-5 catalysts from XPS

Catalyst	Mo/Si	Si/Al	Mo/Si (bulk)	Si/Al (bulk)
Fresh	0.011	17.5	0.028	17.5
Calcined at 700°C	0.059	15.9	0.028	17.5
Used (1 h at 700°C)	0.019	15.1	0.028	17.5

Direct evidence for penetration of molybdenum into the zeolite pores during calcination of the 4% Mo catalysts used here comes from infrared spectra in the ν(OH) region. Fig. 2 compares spectra in this region of the HZSM-5 zeolite with those of the fresh catalyst, catalysts calcined at different temperatures, and a used catalyst. Spectra have been normalized for wafer thickness, so that absolute intensities can be directly compared.

The spectrum of the zeolite without molybdenum shows three characteristic bands in the ν(OH) region: at 3740 cm^{-1} due to external silanol groups, at 3654 cm^{-1} due to AlOH groups associated with extra-framework aluminium, and at 3610 cm^{-1} due to

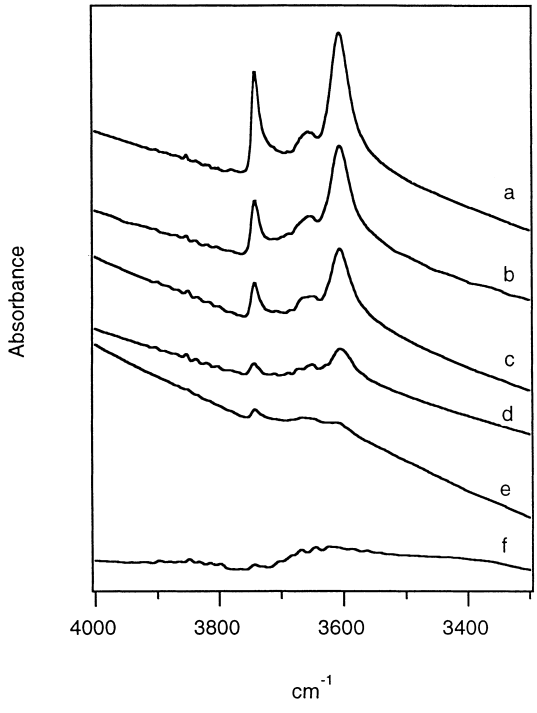

Fig. 2. Infrared spectra of hydroxyl groups (recorded in flowing nitrogen at 100°C) in: (a) HZSM-5; (b) Mo-HSZM-5 as prepared; (c) calcined at 500°C; (d) calcined at 600°C; (e) calcined at 700°C; (f) after reaction. The band at 3610 cm^{-1} is due to Brønsted acid sites.

Brønsted acid sites. Impregnation with ammonium heptamolybdate causes some attenuation of the 3740 cm^{-1} band, confirming location of the initially adsorbed molybdenum on the external surface of the zeolite. Calcination above 500°C causes an attenuation of all three hydroxyl bands; after calcination at 700°C the hydroxyl group concentrations are less than 10% of their initial values. Such an extensive dehydroxylation is not observed when HZSM-5 zeolites are calcined under similar conditions [20].

The loss of hydroxyl groups observed here is more extensive than that reported by Lunsford and coworkers [14]. The molybdenum content of the catalysts is however twice that in [14]. Calcination at 700°C does not totally remove all Brønsted sites from the catalyst; this was confirmed by measurements of the infrared spectra of chemisorbed pyridine, which showed residual Brønsted and Lewis acidity in the calcined catalysts.

Calcination also caused major changes in the ^{29}Si and ^{27}Al NMR spectra of the catalysts. Fig. 3 shows

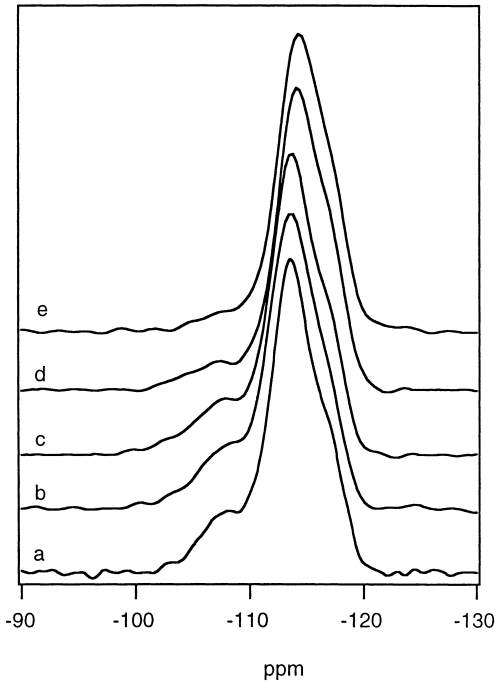

Fig. 3. ^{29}Si MAS NMR spectra of: (a) HZSM-5; (b) Mo-HZSM-5 as prepared; (c) calcined at 500°C; (d) calcined at 700°C; (e) after reaction.

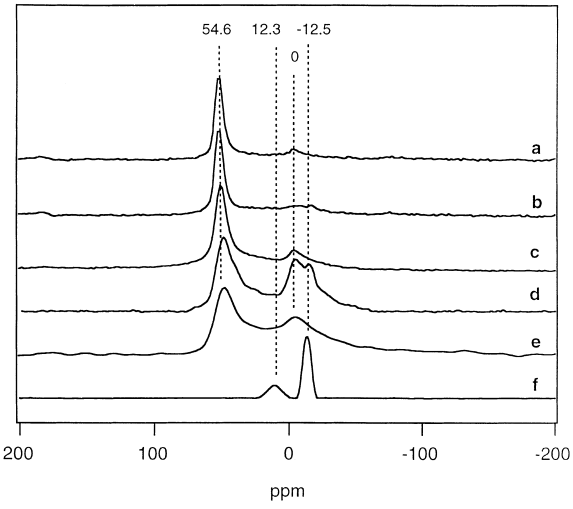

Fig. 4. ^{27}Al MAS NMR spectra of: (a) HZSM-5; (b) Mo-HZSM-5 as prepared; (c) calcined at 500°C; (d) calcined at 700°C; (e) after reaction.

^{29}Si spectra. Calcination causes a diminution in the low field shoulder (108 ppm) due to Si–O–Al, implying loss of aluminium from the zeolite lattice. Similar changes have been seen previously when HZSM-5 zeolites were subjected to high temperature steam treatment, forming extralattice aluminium species [20].

The corresponding ^{27}Al spectra are shown in Fig. 4. Calcination causes the appearance not only of the 0 ppm resonance associated with octahedrally coordinated extralattice aluminium [20], but also an additional signal at higher field (−12 ppm). The spectrum in Fig. 4(f) was measured from a sample of aluminium molybdate ($Al_2(MoO_4)_3$), and shows an identical higher field signal (the broad signal at 12.3 ppm in Fig. 4(f) is due to unreacted alumina in the sample).

The zeolite catalyst contains 2.5 Mo per unit cell. Complete reaction of all molybdenum with lattice aluminium to form aluminium molybdate would consume 1.7 Al per unit cell, or about one third of the total Al content of the zeolite. Quantification of the NMR spectra was not attempted because of uncertainty about the NMR visibility of aluminium species in distorted coordination. Nevertheless, it appears that a major fraction of the molybdenum reacts with lattice aluminium on calcination at high temperatures, destroying Brønsted acid sites and generating extra-

lattice aluminium molybdate species. Reaction also occurs with silanol groups on the external surface and with AlOH sites associated with extralattice aluminium.

Further information about the molybdenum coordination state is obtained from EXAFS measurements at the Mo K-edge. Fig. 5(a) shows the magnitude Fourier transform of the Mo EXAFS from a catalyst as prepared. The radial distribution function contains contributions from at least three coordination shells; the dotted trace is a least squares fit to the data with a model comprising two Mo–O coordination shells and two Mo–Mo coordination shells. Table 2 summarizes the structural parameters derived from least squares fits of the EXAFS data, using a single scattering model.

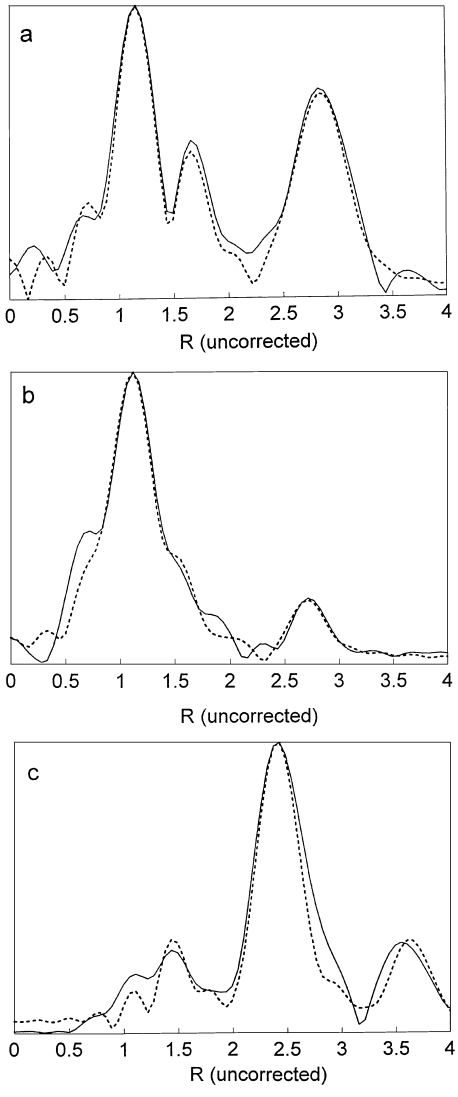

Fig. 5. Magnitude Fourier transforms (not phase corrected) of Mo K-edge EXAFS from: (a) Mo-HZSM-5 as prepared; (b) calcined at 700°C; (c) after reaction. Dotted curves are calculated from the structural parameters in Table 2.

The heptamolybdate ion contains four different Mo–O coordination distances (1.73, 1.99, 2.13 and 2.19 Å), and a corresponding distribution of Mo–Mo distances [23], which makes definitive analysis of the EXAFS difficult [24]. The radial distribution function for the as prepared catalyst does not match exactly with that of ammonium heptamolybdate, suggesting that the species present on the surface of the zeolite after impregnation is not exactly the same as ammonium heptamolybdate. This species is however oligomeric, as judged by the strong contributions to the EXAFS from Mo–Mo coordination shells.

The Mo EXAFS from the calcined catalyst is completely different. The Fourier transform is dominated by a single intense peak corresponding to oxygen nearest neighbours (Fig. 5(b)). Complete fitting of the data required two Mo–O coordination shells, and the weak peak at larger distance corresponds to a single Mo next nearest neighbour at 3.09 Å (Table 2). This radial distribution function is completely different from that of MoO_3 [24], indicating that calcination has caused a dramatic redispersion of molybdenum into the zeolite pores. The simple molybdate anion in Na_2MoO_4 contains four equivalent oxygens at a distance of 1.76 Å [24,25]; the EXAFS of the calcined catalyst is consistent with a similar tetrahedral coordination, albeit with a shorter Mo–O distance.

Fig. 5(c) shows the Fourier transform of the EXAFS from a used catalyst. This is again completely different from that of the calcined catalyst. The radial distribution function is dominated by an intense peak due to Mo–Mo coordination. The weak peak at shorter distance is due to a Mo–C coordination shell, and a second Mo–Mo next nearest neighbour shell is responsible for the third peak at a longer distance. The structural parameters deduced from the EXAFS fit (Table 2) are similar but not identical to those of bulk β Mo_2C (three carbon atoms at 2.09 Å and 12 Mo atoms at 2.96 Å [26]). In particular, the coordination numbers are much lower than those in the bulk

Table 2
EXAFS best fit structural parameters

Sample	Coordination	Distance (Å)	Number	DW (Å^2)[a]
Fresh catalyst	Mo–O	1.68	1.6	0.0035
	Mo–O	2.19	2.8	0.0065
	Mo–Mo	3.14	2.6	0.0098
	Mo–Mo	3.38	4.6	0.0090
Calcined	Mo–O	1.63	4.5	0.0062
	Mo–O	1.91	1.1	0.0019
	Mo–Mo	3.09	1.0	0.0065
Used catalyst	Mo–C	2.00	1.7	0.0011
	Mo–Mo	2.82	3.8	0.0052
	Mo–Mo	4.10	2.5	0.0040

[a]Debye–Waller factor 2σ.

compound, and the distances are slightly shorter. Both of these differences are consistent with a highly dispersed molybdenum carbide phase within the zeolite pores.

3.3. Identity and location of the active phase

The data presented here confirm previous conclusions, principally from XPS [14,15], that a molybdenum carbide phase is formed in active methane conversion catalysts, and that the induction period observed in hydrocarbon production is due to this reaction. There is a clear evidence that during high temperature pretreatment molybdenum initially present on the external surface of the zeolite migrates into the zeolite pores, reacting with Brønsted acid sites to remove aluminium from the lattice and generate, at least in part, an aluminium molybdate phase.

Since the heptamolybdate ion is too bulky to penetrate the zeolite pores, the mobile molybdenum species must be some lower molecular weight form. The nature of this species is under further investigation, but prior literature on the spreading of molybdenum on oxide supports would suggest some form of oxo or hydroxy species [22]. The formation of active catalysts from physical mixtures of Mo_2C and zeolite is not inconsistent with this picture; during calcination in air at 973 K the carbide phase will be fully oxidized and produce similar mobile molybdenum species to the heptamolybdate. Mixtures calcined in helium still contain significant amounts of oxygen which may promote mobility. Solymosi et al. [8] have also reported that partially oxidized Mo_2C mixed with HZSM-5 is active for methane conversion. We have further found that other molybdenum precursors such as molybdenum metal and MoO_3, when mixed with HZSM-5 and calcined in air at 700°C also produce active catalysts [27].

The low activity of unsupported Mo_2C (and the predominance of ethane as a reaction product over this catalyst) further argues against a Mo_2C phase on the external surface of the zeolite being the active species for methane activation. Brønsted acid sites are known to be important in the oligomerization of ethylene to form benzene [7]. The close proximity of a molybdenum carbide phase and residual Brønsted acid sites within the zeolite pores appears to be necessary for optimal activity. The possible role of Lewis acidity should not be discounted, however, given the high concentrations of extralattice Al detected by NMR in used catalysts.

3.4. Prospects for catalyst improvement

From this and previous work on characterization of active catalysts for the methane to benzene reaction, several areas for catalyst improvement can be identified:

1. Achieving maximum dispersion of the active molybdenum phase within the zeolite pores. The spreading of molybdenum into the zeolite is strongly dependant on the calcination conditions, on the particular molybdenum precursor used and

how it is introduced onto the zeolite, and on the aluminium content of the zeolite.

2. The acidity of the zeolite (specifically the concentrations of lattice and extralattice aluminium) is important in the chemistry of both molybdenum dispersion and of the active sites. Optimizing the acidity requires further study of how the active sites are generated.
3. The problem of catalyst deactivation through coke formation is also linked to acidity. Coke formation from hydrocarbons in HZSM-5 is strongly influenced by the density and distribution of acid sites [28]. On the other hand, partial deactivation of the Mo_2C surface by coke deposition may be a necessary prerequisite to ethylene production [14]. Control of catalyst deactivation may require subtle tuning of the catalyst acidity.
4. Given a catalyst containing the optimum dispersion of the molybdenum carbide phase and the requisite number and type of acid sites, further improvement in intrinsic activity may be possible with doping of the catalyst with other transition metals. The initial reports of enhanced performance in bimetallic catalysts [5,10,16,17] suggest that this avenue should be further explored.

Acknowledgements

This work was supported by the Australian Research Council. Access to BL20B at the Photon Factory was provided and funded through the Australian Synchrotron Research Program. We acknowledge also assistance from staff of the Australian National Beam Line Facility.

References

[1] L. Wang, L. Tao, M. Xie, J. Huang, Y. Xu, Catal. Lett. 21 (1993) 35.
[2] F. Solymosi, A. Erdohelyi, A. Szoke, Catal. Lett. 32 (1995) 43.
[3] Y. Xu, S. Liu, L. Wang, M. Xie, X. Guo, Catal. Lett. 30 (1995) 135.
[4] L. Chen, L. Lin, Z. Xu, X. Li, T. Zhang, J. Catal. 157 (1995) 190.
[5] L. Wang, Y. Cu, M. Xie, S. Liu, L. Tao, Stud. Surf. Sci. Catal. 94 (1995) 495.
[6] Y. Xu, Y. Shu, L. Wang, M. Xie, X. Guo, Catal. Lett. 35 (1995) 233.
[7] D. Wang, M. Rosynek, J.H. Lunsford, Topics Catal. 3 (1996) 289.
[8] F. Solymosi, A. Szoke, J. Cserenyi, Catal. Lett. 39 (1996) 157.
[9] A. Szoke, F. Solymosi, Appl. Catal. 142 (1996) 361.
[10] S. Wong, Y. Xu, L. Wang, S. Liu, G. Li, M. Xie, X. Guo, Catal. Lett. 38 (1996) 39.
[11] Y. Xu, W. Liu, S. Wong, L. Wang, X. Guo, Catal. Lett. 40 (1996) 207.
[12] L. Chen, L. Lin, Z. Xu, T. Zhang, X. Li, Catal. Lett. 39 (1996) 169.
[13] S. Wong, Y. Xu, X. Guo, Appl. Catal. A 135 (1996) 7.
[14] D. Wang, J.H. Lunsford, M.P. Rosynek, J. Catal. 169 (1997) 347.
[15] F. Solymosi, J. Cserenyi, A. Szoke, T. Bansagi, A. Oszko, J. Catal. 165 (1997) 150.
[16] Y. Shu, Y. Xu, S. Wong, L. Wang, X. Guo, J. Catal. 170 (1997) 11.
[17] S. Liu, Q. Dong, R. Ohnishi, M. Ichikawa, Chem. Commun., (1997) 1455.
[18] J.S. Lee, L. Volpe, F.H. Ribeiro, M. Boudart, J. Catal. 106 (1987) 125.
[19] W.T. Harrison, A.K. Cheetham, J. Faber, J. Solid State Chem. 76 (1988) 329.
[20] S.M. Campbell, D.M.B. Bibby, J.M. Coddington, R.F. Howe, R.H. Meinhold, J. Catal. 161 (1996) 338.
[21] P. Ellis, H.C. Freeman, J. Synchrotron Radiation 2 (1995) 190.
[22] H. Knozinger, E. Taglauer, in: J. Spivey (Ed.), Catalysis, vol. 10, Royal Society of Chemistry, Cambridge, 1993, p. 1.
[23] E. Shimao, Bull. Chem. Soc. Jpn. 40 (1967) 1609.
[24] C.T. Mensch, J.A. van Veen, B. van Wingerden, M.P. van Dijk, J. Phys. Chem. 92 (1988) 4961.
[25] Structure Reports, vol. 34A, p. 276.
[26] J.S. Lee, L. Volpe, F.H. Ribeiro, M. Boudart, J. Catal. 112 (1988) 44.
[27] J.Z. Zhang, M.A. Long, R.F. Howe, in preparation.
[28] D.M. Bibby, R.F. Howe, G.D. McLellan, Appl. Catal. A 93 (1992) 1.